Role of real-space micromotion for bosonic and fermionic Floquet fractional Chern insulators

Egidijus Anisimovas, Giedrius Žlabys, Brandon M. Anderson, Gediminas Juzeliūnas, and André Eckardt

The role of real-space micromotion for bosonic and fermionic Floquet fractional Chern insulators

Egidijus Anisimovas,[1, 2, *] Giedrius Žlabys,[1, 2] Brandon M. Anderson,[3, 4] Gediminas Juzeliūnas,[1] and André Eckardt[5, †]

[1]*Institute of Theoretical Physics and Astronomy,*
Vilnius University, A. Goštauto 12, LT-01108 Vilnius, Lithuania
[2]*Department of Theoretical Physics, Vilnius University, Saulėtekio 9, LT-10222 Vilnius, Lithuania*
[3]*James Franck Institute, Enrico Fermi Institute and Department of Physics, University of Chicago, Chicago, IL 60637, USA*
[4]*Joint Quantum Institute, University of Maryland, College Park, MD 20742, USA*
[5]*Max-Planck-Institut für Physik komplexer Systeme, Nöthnitzer Straße 38, 01187 Dresden, Germany*
(Dated: 29 May 2015)

Fractional Chern insulators are the proposed phases of matter mimicking the physics of fractional quantum Hall states on a lattice without an overall magnetic field. The notion of Floquet fractional Chern insulators refers to the potential possibilities to generate the underlying topological band-structure by means of Floquet engineering. In these schemes, a highly controllable and strongly interacting system is periodically driven by an external force at a frequency such that double tunneling events during one forcing period become important and contribute to shaping the required effective energy bands. We show that in the described circumstances it is necessary to take into account also third order processes combining two tunneling events with interactions. Referring to the obtained contributions as micromotion-induced interactions, we find that those interactions tend to have a negative impact on the stability of fractional Chern insulating phases and discuss implications for future experiments.

I. INTRODUCTION

Chern insulators[1] form a primary and most widely studied class of more general topological insulators,[2,3] proposed in condensed matter settings, in particular, heterostructures[4–6] and graphene.[7,8] They are characterized by topological Bloch bands, that is, energy bands that give rise to a quantized Hall conductivity, when filled completely in a band-insulating state. The contribution of each band to the Hall conductivity is identified by an integer topological index, known as the Chern number. From this point of view topological bands can be thought of as generalizations of the Landau level.[9] However, they can be realized in a broad variety of physical settings independent of the requirement to have electrically charged particles coupled to an intense uniform magnetic field. The analogy between a Landau level and a Chern band hints at the idea of *fractional* Chern insulators (FCI).[10–17] In this case, in addition to an isolated energy band characterized by a nonvanishing integral of the Berry curvature (which defines the Chern number) one also needs strong particle interactions to form the collective states analogous to (and presumably richer than) the usual fractional quantum Hall states.

It turned out that a powerful method to produce the desired topological bandstructures is *Floquet engineering.* This form of quantum engineering is based on the fact that the dynamics of a time-periodically driven quantum system, a so-called Floquet system, is (apart from a periodic micromotion) captured by a time-independent effective Hamiltonian. Properties of the effective Hamiltonian can be engineered by tailoring a suitable driving protocol. Floquet engineering has been very suc-

cessfully applied to quantum systems of ultracold atoms in periodically driven optical lattices.[18–35] These systems are particularly suitable for such control schemes due to their high degree of isolation from the environment and versatile possibilities for controlling parameters in a time-dependent fashion during the experiment. In recent years, several schemes have been proposed where periodic driving is employed for the realization of topologically nontrivial effective bandstructures in lattice systems, which in the absence of the driving are topologically trivial. These schemes can be divided into two classes: (i) methods working at high driving frequencies[26,28,31,32,36–39] and relying on averaging the driven Hamiltonian over a period, and (ii) methods working at intermediate driving frequencies[34,40–43] and going beyond the time-averaged description. For the latter, the term *Floquet topological insulator* has been coined.[44,45]

The high-frequency schemes have been proposed and implemented in the context of ultracold atomic quantum gases in optical lattices[26–32,36,38] and trapped ions.[37] Here, static and time-periodic potentials are combined in such a way that the wavefunction acquires time-periodic relative phases on neighboring lattice sites. When averaged over one driving period, these phases resemble the nontrivial phases induced by a magnetic field. These schemes work at large frequencies, since it is assumed that the driving period T determining the phase modulation is short compared to the tunneling time. The topologically nontrivial effective bandstructure of such a system has been recently probed in a square optical lattice.[38]

The Floquet topological insulator schemes[40,41,44] were originally proposed in the context of condensed matter

systems, considering irradiated graphene[40,46–48] or semi-conductor heterostructures, and are based on a different principle. Here, the effective Hamiltonian acquires new terms that describe tunneling between next-nearest neighbors and open a topological gap in the bandstructure. These new terms are related to second-order processes, where a particle tunnels twice during one driving period. Obviously they are significant only at intermediate driving frequencies, with the driving period being comparable to (or at most moderately shorter than) the tunneling time. This is the regime where particles undergo a significant periodic real-space micromotion in response to the driving. Signatures of such Floquet topological bandstructures have been observed in optical waveguides[43] and with ultracold fermionic atoms in a shaken honeycomb lattice.[34]

As a natural next step, recently it has been proposed to stabilize a fractional topological insulator phase in such a Floquet topological bandstructure, referred to as the Floquet fractional Chern insulator.[17] The scheme is based on fermions in a circularly driven honeycomb lattice, which acquires a topologically nontrivial effective bandstructure.[40] For their analysis, the authors employed a high-frequency approximation[49–51] of the effective Hamiltonian, including terms up to the second order. On this level of approximation, the nontrivial tunneling terms opening the topological single-particle bandgap are included, but no corrections to the interaction terms appear.[51,52] The exact diagonalization of the approximate effective Hamiltonian for small systems suggested that a topologically ordered state can be stabilized at a band filling of 1/3.

The realization of such a topologically ordered many-body Floquet state is, however, challenged in various ways. One difficulty concerns the preparation of the state both in open condensed matter systems as well as in isolated cold-atom systems. As a consequence of the coupling to a bath, open Floquet systems will assume steady states, which are generally quite different from equilibrium states.[53–60] In turn, an isolated Floquet system has to be prepared in the desired state using smooth, effectively adiabatic[61] parameter variations starting from the undriven ground state (or from a low-temperature state close to it). A second concern is that excitations to higher-lying bands, which are not included in the tight-binding description, via multi-"photon" transitions may become relevant on the time scale of the experiment; see Ref. [62] for a recent experimental investigation of such processes. Finally, also the impact of interactions beyond the second-order high-frequency approximation can be a relevant issue. Such "residual" interactions enter on two different levels, they cause heating and they lead to higher-order corrections to the approximate effective Hamiltonian. Interaction-induced heating corresponds to processes that can be viewed as the resonant creation of collective excitations of the effective Hamiltonian in high-frequency approximation. Such processes are not captured within the high-frequency expansion,

they indicate that such an expansion cannot be expected to converge for an interacting system[51] and they are expected to eventually drive the system towards an infinite-temperature regime.[63,64] A perturbative argument suggests that the rate of such detrimental heating will decrease exponentially with increasing driving frequency (as the order in which the corresponding processes appear increases with the driving frequency).[61] Apart from heating, interactions will also lead to corrections appearing in higher orders of the high-frequency expansion, with the leading correction appearing in third order.[51]

In this paper we investigate the impact of leading interaction correction to the approximate effective Hamiltonian. We do not address the issues of preparation and heating due to either multi-photon interband transitions or the resonant excitation of collective excitations. While it is rather clear that heating is a detrimental effect, it is an interesting question without an *a priori* obvious answer, whether the interaction corrections will tend to stabilize or to destabilize a Floquet fractional Chern insulator state. Even though the leading interaction corrections appear in third order only, they are still relevant for the required intermediate driving frequencies. First of all, if interactions are strong compared to tunneling, a third-order interaction correction can be comparable to a second-order kinetic term. And second, because the correction has to be compared with the tiny manybody gap that protects the ground-state manifold of the effective Hamiltonian from excited states. The origin of the interaction corrections to be investigated here is a significant real-space micromotion at intermediate driving frequencies. A particle at a certain lattice site will explore also neighboring sites during one driving period. This real-space micromotion generates new effective interactions at distances longer than those of the bare interactions characterizing the undriven model.

For our study, we use exact diagonalization for small systems, taking into account the leading interaction correction. In addition to a model of spin-polarized fermions with nearest-neighbor interactions (which includes the ground states found in Ref. [17]) we also consider a system of spinless bosons with onsite interactions. The latter is particularly interesting for experiments with ultracold atoms in shaken optical lattices, and is typically governed by onsite interactions. In both models we find that taking into account interaction corrections tends to destabilize topologically ordered fractional Chern states. Thus the realization of Floquet fractional Chern insulator states seems rather challenging and it might be more promising to consider high-frequency schemes or schemes involving internal degrees of freedom.[35,65]

The bulk of the presented material is split between two large sections, each subdivided into three subsections. Sec. II discusses the model, starting with the description of the lattice and the shaking protocol, and later proceeding to the Floquet analysis, the underlying single-particle problem and the role of interactions. Section III focuses on results, and encompasses description of the numerical

procedure, the obtained manybody bandstructures and quasihole spectra, characterizing the fractional Chern insulating states. Finally, we conclude with a brief summarizing Sec. IV.
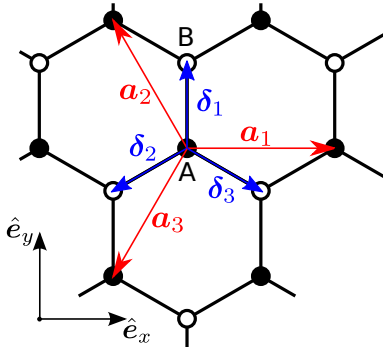
II. MODEL

FIG. 1. Honeycomb lattice as a triangular Bravais lattice with a two-site basis. The inequivalent sites A and B are marked with filled and open dots, respectively. Nearest neighbors are connected by the vectors $\boldsymbol{\delta}_\mu$, while the set of next-nearest neighbor vectors $\boldsymbol{a}_j$ also defines the elementary translations.

The model proposed by Grushin et al.[17] is based on a honeycomb lattice sketched in Fig. 1, and consisting of two intertwined triangular sublattices A and B. For the sake of further reference, Fig. 1 defines the vectors

$$\boldsymbol{\delta}_1 = a\,\hat{\boldsymbol{e}}_y, \qquad \boldsymbol{\delta}_{2|3} = \mp\frac{\sqrt{3}}{2}a\,\hat{\boldsymbol{e}}_x - \frac{1}{2}a\,\hat{\boldsymbol{e}}_y, \qquad (1)$$

connecting a given site A to its three nearest neighbors (NN) on sublattice B, with a denoting the nearest-neighbor distance, and $\hat{\boldsymbol{e}}_{x,y}$ being the unit coordinate vectors. Likewise, the vectors $\pm\boldsymbol{a}$ with

$$\boldsymbol{a}_1 = \sqrt{3}a\,\hat{\boldsymbol{e}}_x, \qquad \boldsymbol{a}_{2|3} = -\frac{\sqrt{3}}{2}a\,\hat{\boldsymbol{e}}_x \pm \frac{3}{2}a\,\hat{\boldsymbol{e}}_y, \qquad (2)$$

connect a given site of either type to its six next-nearest neighbors (NNN) belonging to the same sublattice. Note that NNN hopping transitions naturally separate into two classes. Transitions starting from a site A (resp. B) in the direction of $\boldsymbol{a}_j$ correspond to counterclockwise (resp. clockwise) motion around the hexagonal cell, and the opposite statement applies to transitions along $-\boldsymbol{a}_j$. The vectors $\boldsymbol{a}_1$ and $\boldsymbol{a}_2$ are also taken to define the Bravais lattice $\boldsymbol{r} = n_1\boldsymbol{a}_1 + n_2\boldsymbol{a}_2$, while $\boldsymbol{a}_3 = -\boldsymbol{a}_1 - \boldsymbol{a}_2$ is linearly dependent.

The honeycomb lattice is subjected to a circular time-periodic force of fixed magnitude F, whose direction rotates in the (x-y) lattice plane at a constant frequency ω, thus

$$\boldsymbol{F}(t) = F\sin\omega t\,\hat{\boldsymbol{e}}_x - F\cos\omega t\,\hat{\boldsymbol{e}}_y. \qquad (3)$$

This force results from either the circular shaking[23,34,66] of an optical lattice or, in the case of charged particles, from irradiation by circularly polarized light.[40] A suitable gauge transformation[35,51] (corresponding to transition to the comoving frame of reference) restores the translational invariance of the Hamiltonian, which is then represented in the tight-binding form as a sum of the time-periodic kinetic and time-independent interaction parts,

$$\hat{H}(t) = \hat{H}_{\text{kin}}(t) + \hat{H}_{\text{int}}. \qquad (4)$$

The kinetic Hamiltonian reads

$$\hat{H}_{\text{kin}}(t) = -\sum_{i\in A}\sum_{\mu=1}^{3} J_\mu(t)\,\hat{a}^\dagger_{i+\mu}\hat{a}_i + h.c., \qquad (5)$$

here, the operator $\hat{a}^\dagger_i$ creates a spinless particle (fermion or boson) on lattice site i. The index μ labels the three distinct directions connecting any given site of sublattice A to its nearest neighbors belonging to sublattice B, and denoted by the shorthand label "$i+\mu$" with $i \in A$. Extension to spinful particles, although not necessary for the purposes of the current presentation, is straightforward. Equation (5) describes the nearest-neighbor tunneling kinetics. The tunneling matrix elements along the three different directions acquire their time dependence due to the circular driving, and thus are time-periodic with uniformly distributed relative phases, i.e.,

$$J_\mu(t) = J(t - \varphi_\mu/\omega), \quad \text{with} \quad \varphi_\mu = \frac{2\pi}{3}(\mu - 1). \qquad (6)$$

Having in mind applications to ultracold atoms in a circularly shaken optical lattice or graphene electrons irradiated by circularly polarized light, we write

$$J(t) = J\exp(i\alpha\sin\omega t), \qquad (7)$$

with

$$\alpha = \frac{Fa}{\hbar\omega} \qquad (8)$$

denoting the dimensionless shaking strength.

In bosonic quantum gases contact interactions may be assumed, therefore, the interaction Hamiltonian is written in the standard Bose-Hubbard form

$$\hat{H}^{(\text{b})}_{\text{int}} = \frac{U}{2}\sum_{i\in A,B}\hat{n}_i\left(\hat{n}_i - 1\right), \qquad (9)$$

with the operator $\hat{n}_i = \hat{a}^\dagger_i\hat{a}_i$ measuring the particle number on a given site. In contrast, for spinless fermions the onsite interaction term vanishes due to the Pauli exclusion principle, and repulsion between pairs of particles occupying neighboring sites must be taken into account, thus

$$\hat{H}^{(\text{f})}_{\text{int}} = V\sum_{i\in A}\sum_{\mu=1}^{3}\hat{n}_i\hat{n}_{i+\mu}. \qquad (10)$$

Therefore, depending on the particle statistics, we model the interactions using one of the two alternative forms given by either Eq. (9) or (10). Note also, that in both cases the interaction Hamiltonian depends only on densities, and thus remains static also in the presence of periodic driving. Our choice of treating spinless, that is spin-polarized, fermions is motivated not only by simplicity, but also by the observation of Ref. 17 that the relevant Floquet fractional Chern insulating states are ferromagnetic.

A. Floquet analysis

As discussed in the Introduction, Floquet Chern insulators by construction require intermediate driving frequencies on the order of the tunneling strength or just moderately larger. This observation identifies the dimensionless inverse shaking frequency

$$\beta = \frac{J}{\hbar\omega} \tag{11}$$

as the series-expansion parameter that classifies the successive contributions to the effective Hamiltonian, and in turn, to the ensuing physics. In further study we

focus on the interval $0.1 \leqslant \beta \leqslant 0.5$. At the lower limit of this range, one crosses over to the high-frequency regime where the effective Hamiltonian is adequately represented by the time average of the driven Hamiltonian while the relevance of higher-order contributions fades away. In the opposite limit, for values of β exceeding one-half the representation of the effective Hamiltonian in terms of a β-series expansion in no longer reliable.

A powerful description of periodically driven quantum systems[49–51,67,68] relies on the factorization of the quantum-mechanical evolution operator according to

$$\hat{U}(t_2, t_1) = \hat{U}_F(t_2)\,e^{-i\hat{H}_F(t_2-t_1)/\hbar}\,\hat{U}_F^\dagger(t_1), \tag{12}$$

thus separating micromotion described by the time-periodic unitary micromotion operator $\hat{U}_F(t)$ from the long-term dynamics captured by the effective Hamiltonian $\hat{H}_F$. A consistent high-frequency approximation to the effective Hamiltonian $\hat{H}_F$ is constructed in Refs. 49, 51, and 67 following different approaches and resulting in equivalent[69] series representation in powers of ω^{-1}

$$\hat{H}_F = \hat{H}_F^{(1)} + \hat{H}_F^{(2)} + \hat{H}_F^{(3)} + \cdots, \tag{13}$$

where

$$\hat{H}_F^{(1)} = \hat{H}_0, \tag{14a}$$

$$\hat{H}_F^{(2)} = \sum_{m=1}^\infty \frac{1}{m\hbar\omega}\left[\hat{H}_m, \hat{H}_m^\dagger\right], \tag{14b}$$

$$\hat{H}_F^{(3)} = \frac{1}{2(\hbar\omega)^2}\sum_{m=1}^\infty \frac{[\hat{H}_m,[\hat{H}_0,\hat{H}_m^\dagger]]}{m^2} + \frac{1}{3(\hbar\omega)^2}\sum_{\substack{m,m'=1\\m'\neq m}}^\infty \frac{[\hat{H}_{-m'},[\hat{H}_{m'-m},\hat{H}_m]] - [\hat{H}_{m'},[\hat{H}_{-m'-m},\hat{H}_m]]}{mm'} + h.\,c., \tag{14c}$$

are expressed in terms of Fourier components of the driven Hamiltonian

$$\hat{H}(t) = \sum_{m=-\infty}^\infty \hat{H}_m\,e^{im\omega t}. \tag{15}$$

It is useful to note the hermiticity condition $\hat{H}_{-m} = \hat{H}_m^\dagger$. The leading terms of the corresponding expansion of $\hat{U}_F(t)$ can be found in Ref. 51. Note that the high-frequency expansion of $\hat{U}_F(t)$ and $\hat{H}_F$ can be related to the Magnus expansion, as described in Refs. 49 and 51.

For the purposes of the current application, the general expressions (14) can be simplified in two aspects. First, we note that the time dependence of the driven Hamiltonian stems entirely from the time-dependent hopping amplitudes described by the Fourier expansion

$$J_\mu(t) = \sum_{m=-\infty}^\infty J\mathcal{J}_m(\alpha)\,e^{-im\varphi_\mu}\,e^{im\omega t}, \tag{16}$$

with Bessel functions of the first kind (and order m), denoted here by $\mathcal{J}_m$. Anticipating moderate shaking strengths α [see Table I] we note that the Fourier series of the Hamiltonian converge very fast since contributions originating from the mth harmonic with $m > 0$ include a prefactor $\mathcal{J}_m^2(\alpha) \sim \alpha^{2|m|}$ (see Fig. 2). Further noting that all harmonics contribute with the same operator form and thus cannot induce qualitative changes, we truncate the Fourier expansion and include only the terms with $|m| \leqslant 1$. Consequently, non-zero Fourier components of the driven Hamiltonian are

$$\hat{H}_0 = \hat{H}_{\text{int}} - \sum_{i\in A}\sum_\mu J\mathcal{J}_0(\alpha)\left[\hat{a}_{i+\mu}^\dagger\hat{a}_i + \hat{a}_i^\dagger\hat{a}_{i+\mu}\right], \tag{17a}$$

$$\hat{H}_{\pm1} = \mp\sum_{i\in A}\sum_\mu J\mathcal{J}_1(\alpha)\,e^{\mp i\varphi_\mu}\left[\hat{a}_{i+\mu}^\dagger\hat{a}_i - \hat{a}_i^\dagger\hat{a}_{i+\mu}\right], \tag{17b}$$

where the interaction Hamiltonian $\hat{H}_{\text{int}}$ is given by either Eq. (9) or Eq. (10) for bosonic and fermionic systems, respectively.
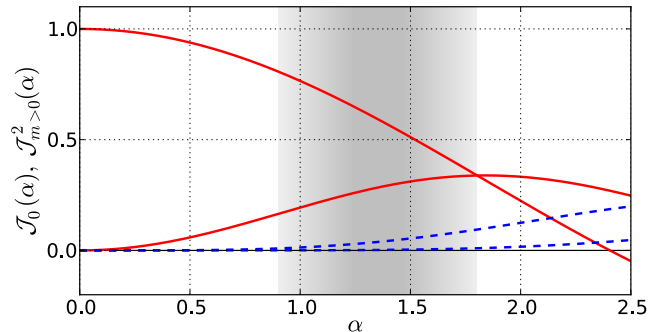

FIG. 2. Comparison of the importance of various Fourier harmonics. The shaded background shows the range of the dimensionless shaking amplitudes α considered in the calculations. The red lines depict the behavior of $\mathcal{J}_0(\alpha)$ and $\mathcal{J}_1^2(\alpha)$, setting the scale of, respectively, the static components of the Hamiltonian and the first harmonic. The dashed blue lines show the behavior of the (omitted) subleading contributions $\mathcal{J}_{2,3}^2(\alpha)$.

Secondly, focusing on the interplay of micromotion and interactions we take into account the leading third-order interaction correction while neglecting purely kinetic terms of third order. Thus, the expansion of the effective Hamiltonian considered in our work reads

$$\hat{H}_F^{(1)} = \hat{H}_0, \tag{18a}$$

$$\hat{H}_F^{(2)} = \frac{1}{\hbar\omega}\left[\hat{H}_1, \hat{H}_1^{\dagger}\right], \tag{18b}$$

$$\hat{H}_F^{(3)} = \frac{1}{2(\hbar\omega)^2}\left[\hat{H}_1, \left[\hat{H}_{\text{int}}, \hat{H}_1^{\dagger}\right]\right] + h.c.. \tag{18c}$$

B. Single-particle spectrum

The first-order contribution to the effective Hamiltonian given by Eq. (18a) is obtained by averaging the driven Hamiltonian $\hat{H}(t)$ over a period. This leads to the result given by Eq. (17a) and featuring the well known renormalization of NN hopping amplitude according to the prescription $J \to J\mathcal{J}_0(\alpha)$, which has been extensively exploited to demonstrate a number of interesting physical effects in cold atom settings, including the superfluid-Mott insulator phase transition.[18,21]

The second-order Floquet contribution is expressed by the commutator in Eq. (18b), and physically corresponds to two subsequent tunneling processes of a particle during one driving period. The basic commutation relation $[\hat{a}_k^{\dagger}\hat{a}_\ell, \hat{a}_m^{\dagger}\hat{a}_n] = \delta_{\ell m}\hat{a}_k^{\dagger}\hat{a}_n - \delta_{kn}\hat{a}_m^{\dagger}\hat{a}_\ell$ is valid for particles of either statistics and combines two successive NN tunneling events into an effective NNN transition. Thus,[70]

$$\hat{H}_F^{(2)} = -\sum_{\langle\langle ij\rangle\rangle} J_{\langle\langle ij\rangle\rangle}^{(2)} \hat{a}_i^{\dagger}\hat{a}_j, \tag{19}$$

with the sum running over all next-nearest neighbor connections, and

$$J_{\langle\langle ij\rangle\rangle}^{(2)} = \pm\mathrm{i}\sqrt{3}\,\beta J\mathcal{J}_1^2(\alpha). \tag{20}$$

The plus (minus) sign applies to clockwise (counterclockwise) transitions around the hexagonal unit cell. Note that NNN transitions in Eq. (19) are characterized by purely imaginary amplitudes.

The role of the second-order contribution to the effective Hamiltonian in Floquet engineering is to open topological gaps in the single-particle spectrum. This produces the Haldane model[1] using driven honeycomb lattices.[23,34,35,41,66] Since the possibility to stabilize the FCI phases is the ultimate question of this work, one is interested in starting from a favorable single-particle bandstructure characterized by relatively flat bands (at least in a part of the Brillouin zone) that are separated by large energy gaps. As noted previously,[17] this requirement leads to a constraint relating the shaking amplitude α to the inverse frequency β. The detailed discussion of this matter is delegated to the Appendix A, with the conclusion that the relative strengths of NNN and NN transition amplitudes must be close to the ratio

$$\frac{\beta\,\mathcal{J}_1^2(\alpha)}{\mathcal{J}_0(\alpha)} = \frac{1}{4\sqrt{6}}. \tag{21}$$

Thus, for any given value of the inverse shaking strength β, the constraint (21) defines the corresponding "nominal" value of the driving strength α_0 which optimizes the single-particle bandstructure. Let us stress, however, that thus defined value α_0 should be regarded more as *representative* rather than precisely defined optimal value. We verified that moderate deviations of the value of α from α_0 do not change the results qualitatively. Thus, focusing on a single value helps to reduce the dimensionality of the parameter phase space.

C. Role of interactions

A cornerstone of the present contribution is the argument that the real-space micromotion couples to the particle interactions through Eq. (18c), which leads to the generation of new (and modification of existing[71]) interaction terms, and in particular, influences the formation and stability of FCI phases. Possible interplay of micromotion and interactions was previously discussed[72–74] basing on approximation schemes related to the Magnus expansion.[75] The obtained terms are proportional to the inverse driving frequency and typically offer a clear physical interpretation (such as the density-assisted tunneling). However, as discussed in Ref. 51 as well as Ref. 49, these terms do not influence the spectrum within the order of the approximation.

In the present context of circularly shaken honeycomb lattices, micromotion-induced interaction corrections were analyzed and the physical nature of the additional terms was identified in Ref. 51. Following this

work and specializing to moderate driving amplitudes, such that Fourier components $|m| \leqslant 1$ are sufficient, we observe that the overall strength of these terms is set by the prefactor

$$\frac{U J^2 \mathcal{J}_1^2(\alpha)}{(\hbar\omega)^2} = U\beta^2 \mathcal{J}_1^2(\alpha) = \eta U. \tag{22}$$

Here we introduced the dimensionless quantity $\eta = \beta^2 \mathcal{J}_1^2(\alpha)$ as a natural measure of the relative strength of micromotion-induced interactions with respect to the bare onsite repulsion. The five additional contributions for bosons with contact interactions read:

$$\hat{H}_F^{(3,\text{b})} = -2z\eta U \sum_i \hat{n}_i (\hat{n}_i - 1) \tag{23a}$$

$$+ 4\eta U \sum_{\langle ij \rangle} \hat{n}_i \hat{n}_j \tag{23b}$$

$$+ 2\eta U \sum_{\langle ij \rangle} \hat{a}_i^\dagger \hat{a}_i^\dagger \hat{a}_j \hat{a}_j \tag{23c}$$

$$- \tfrac{1}{2}\eta U \sum_{\langle ijk \rangle} \hat{a}_i^\dagger (4\hat{n}_j - \hat{n}_i - \hat{n}_k)\hat{a}_k \tag{23d}$$

$$- \tfrac{1}{2}\eta U \sum_{\langle ijk \rangle} \left(\hat{a}_j^\dagger \hat{a}_j^\dagger \hat{a}_i \hat{a}_k + h.c. \right). \tag{23e}$$

Here, $z = 3$ is the coordination number (the number of nearest neighbors), and the sums are taken, respectively, over the lattice sites i, all directed NN links $\langle ij \rangle$, and all directed three-site strings $\langle ijk \rangle$ with i and k being next-nearest neighbors connected via an intermediate site j. The physical interpretation of the obtained terms is as follows: (a) reduction of the onsite interaction strength, (b) nearest-neighbor density-density interaction, (c) pair tunneling, (d) density-assisted tunneling between NNN sites, and (e) cotunneling of pairs of particles into (from) a given site from (into) two *distinct* nearest neighbors. While for fermionic particles the corresponding analysis becomes more involved and is not presented here, we emphasize that the general comparison of the relative importance of micromotion-induced interactions and the definition of η remain unchanged except for the replacement of onsite repulsion energy U with NN repulsion energy V.

In general, the overall scale of the micromotion-induced interactions (i. e., the value of η) is not an independent parameter but is set by the driving frequency (β) and strength (α). Since the preferred value of the driving strength α_0 is in turn fixed by the flat-band condition, all in all, we have to consider a one-dimensional cut through the apparently three-dimensional parameter space (α, β, η). The characteristic range of values is summarized in Table I.

As explained previously, the eligible values of the dimensionless inverse shaking frequencies β are constrained to

TABLE I. Numerical values of parameters used in calculation.

$\beta = 0.1$	$\alpha_0 = 1.814$	$\eta = 0.003$
$\beta = 0.2$	$\alpha_0 = 1.391$	$\eta = 0.011$
$\beta = 0.3$	$\alpha_0 = 1.153$	$\eta = 0.021$
$\beta = 0.4$	$\alpha_0 = 1.004$	$\eta = 0.031$
$\beta = 0.5$	$\alpha_0 = 0.900$	$\eta = 0.041$

an interval consistent with the physical setting. One can see, that the corresponding values of the shaking strength α_0 are also restricted to an interval where: (i) the single-particle bands do not collapse as the zeros of the zeroth-order Bessel function are avoided, and (ii) the employed truncation of the Fourier series is indeed valid.

Turning to the last column displaying the values of η, one observes that the relative contribution of micromotion-induced corrections to the overall strength of interactions is limited to a few percent. However, these low values should not be taken as a proof that micromotion-induced interactions may be neglected. In fact, in the context of the stabilization of FCI phases, their importance should be measured with respect to manybody gaps separating the ground-state manifold, and judged by their impact on the FCI stability diagram. As we will see shortly, micromotion-induced interactions may indeed be significant and tend to destabilize fractional Floquet states.

III. RESULTS

A. Numerical procedure

To gain specific insights into the impact of micromotion on the formation and stability of FCI phases we performed a numerical exact-diagonalization study of periodically driven honeycomb lattices. The most stable fractional quantum Hall-like states are expected to form at filling fractions $\nu = \frac{1}{3}$ for fermions and $\nu = \frac{1}{2}$ for bosons. Therefore, our numerical modeling mostly focused on finite systems of $N_p = 8$ spinless fermions (resp. bosons) moving on a lattice containing $N_1 \times N_2 = 6 \times 4$ (resp. $N_1 \times N_2 = 4 \times 4$) elementary two-site cells. While comparisons with results obtained for larger systems were used for consistency checks and validation of the general conclusions, the bulk of calculations was performed on moderate eight-particle systems. Keeping the system size relatively small allowed for looping over a dense grid in the parameter phase space defined by the aforementioned inverse driving frequency β and the interaction strength U or V, as well as the auxiliary phases γ_1 and γ_2 introduced through twisted boundary conditions[76] in the two primary lattice directions. Twisting the boundary conditions in the ith direction by a phase factor $e^{i\gamma_i}$ represents the insertion of the dimensionless flux γ_i, and leads to the variation of the calculated energy levels, which is com-

monly referred to as the spectral flow. The formation of the topological order is signaled (however, not rigorously proven) by the formation of the ground-state manifold (GSM) consisting of ν^{-1} quasidegenerate states that re-arrange under the spectral flow but remain isolated from the other states by a finite manybody gap.[12,15]

In view of the translational invariance, restored in the finite system by the cyclic boundary conditions, our cal-culations are performed in the reciprocal (or quasimo-mentum) $\boldsymbol{k}$-space. The finite geometry of the lattice im-poses a discreet grid of $N_1 \times N_2$ permissible values in a Brillouin zone (BZ) for both single-particle and total quasimomenta. The diagonalizations can be performed separately at each total quasimomentum $\boldsymbol{k}$ thus signifi-cantly reducing the size of the problem. To quote a spe-cific example, in the 8-fermion system the dimensionality of the Hilbert space reduces from $24!/(16!\,8!) \approx 7.35 \times 10^5$ to just above 3×10^4 when translational invariance is taken into account. The $\boldsymbol{k}$-space points belonging to a single Brillouin zone are labelled by integer pairs (k_1, k_2) with $k_1 \in [0, N_1 - 1]$ and $k_2 \in [0, N_2 - 1]$ or, equivalently, by a single index $K = k_1 + N_1 k_2$ with $K \in [0, N_1 N_2 - 1]$. The total quasimomentum sectors at which the FCI states will form are predicted by a simple counting rule[12] whose validity in the present case is indeed confirmed by the actual numerical results. Thus, for eight fermions, the FCI states form at $K = \{0, 2, 4\}$, while for eight bosons one finds two states at $K = 0$.

Following previous works that demonstrated the potential existence of FCI phases in various lattice models[10–14] with strong particle interactions, we use the customary band projection technique (see, e.g., reviews in Refs. 15 and 16 for an extensive discussion). Thereby, only processes in the relevant single-particle band are in-cluded, while the interband scattering events as well as processes related to the remaining band are neglected. Note however, that we *do not* flatten the bandstructure which is another standard tool of the trade.[11,15] The rea-son for this choice of techniques is the following: In con-trast to models based on energy bands featuring weak dispersion throughout the Brillouin zone, we deal here with single-particle bands that are in general dispersive, however, the upper (resp. lower) single-particle band de-velops a relatively flat section at the bottom (resp. top) where also the Berry curvature is the largest. In this sit-uation, band flattening would lead to an essential distor-tion of the model and therefore must be avoided. When modeling fermionic systems we adopt the approach of Ref. 17 and consider a gas at the density of 4 particles per 3 elementary cells. This produces a completely filled, and thus inert, lower band plus a partially filled upper band with particles predominantly concentrating in the flat section. Therefore, projecting onto the upper band we are able to focus on the physics at the effective filling factor $\nu = \frac{1}{3}$. Proceeding to bosonic systems we envi-sion a gas at the density of one particle per 2 elementary cells, and employ projection onto the lower single-particle band.

B. Manybody topological gap

As discussed previously, the parameter phase space to be explored is essentially two-dimensional, and is spanned by the inverse driving frequency $\beta = J/\hbar\omega$, and the particle repulsion strength. It is natural to measure the interaction energies with respect to the basic hop-ping amplitude, thus introducing the corresponding di-mensionless quantities

$$u = \frac{U}{J}, \quad \text{and} \quad v = \frac{V}{J}, \tag{24}$$
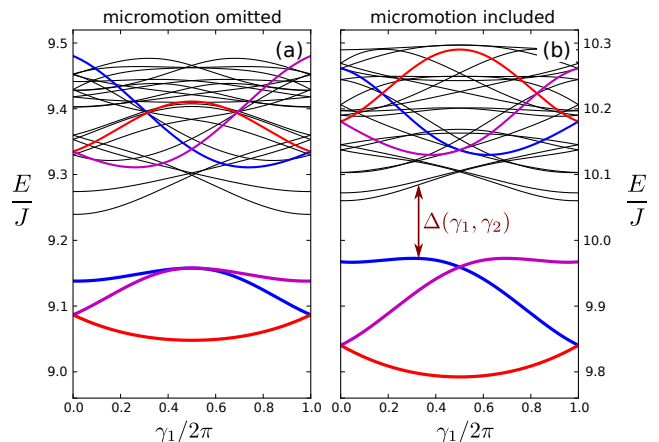
for bosonic and fermionic systems, respectively.

FIG. 3. Typical energy spectra of the driven honeycomb lattice with micromotion-induced interactions ignored [panel (a)], and taken into account [panel (b)] plotted versus the aux-iliary flux γ_1 inserted along the first (commensurate) lattice direction. Here, the energies of manybody states in the eight-fermion system numerically calculated at $\beta = 0.3$, $v = 5$, and $\gamma_2 = 0$ are shown. Colored (resp. black) lines denote the states in the ground-state manifold (resp. other) total quasimomen-tum sectors, and two lowest-energy states of each quasimo-mentum sector are included. The dark red arrow illustrates the definition of the *local* manybody gap referred to in the text.

Figure 3 shows the calculated energy spectra of eight-fermion manybody states in the form of spectral flows along the first (commensurate) direction. The three states belonging to the expected FCI total quasimomen-tum sectors $K = \{0, 2, 4\}$ are plotted in color while the remaining states are plotted in black. The insertion of the artificial flux γ_1 defining the twisted boundary con-ditions makes the three states in the GSM interchange and reconnect to their partners at the opposite bound-ary of the manybody Brillouin zone (MBZ). The plot is obtained by setting $\beta = 0.3$, $v = 5$, and $\gamma_2 = 0$. In the left panel, the micromotion strength η is artificially set to zero (as would happen in a calculation omitting the presence of real-space micromotion). The nearly de-generate states in the GSM stay protected from the ex-cited states by a manybody gap, and their total Chern

number obtained from sampling over the whole MBZ $(\gamma_1, \gamma_2) \in [0, 2\pi) \times [0, 2\pi)$ sums up to unity with numerical precision. The right panel shows the realistic situation where coupling between micromotion and interactions is duly taken into account up to the third order. While the topological nature of the lowest-energy manifold and the manybody gap persist, its width is reduced and the energy spread of the states in the GSM is now considerably larger. These observations serve as an early hint that the interplay of micromotion and interactions is significant, and may indeed have a detrimental role on the stability of the Floquet fractional Chern insulating phases.

Referring to Fig. 3, we also take the opportunity to give a precise definition to the notion of the manybody gap to be used in presentation of further results. Since calculations are performed looping over the manybody Brillouin zone we first define the *local* (that is, corresponding to fixed values of $\gamma_{1,2}$) dimensionless manybody gap

$$\Delta(\gamma_1, \gamma_2) = \frac{1}{J} \left[\min_{\text{not in GSM}} E(\gamma_1, \gamma_2) - \max_{\text{GSM}} E(\gamma_1, \gamma_2) \right], \tag{25}$$

as the energy difference between the highest state belonging to GSM and the lowest-lying state outside the GSM measured in units of J. Thus, $\Delta(\gamma_1, \gamma_2)$ is positive when an isolated ground state manifold is formed and negative when the states in the ground-state manifold mix with the remaining states. The overall manybody gap is then obtained by minimizing the local manybody gap over the entire MBZ, thus

$$\Delta = \min_{\text{MBZ}} \Delta(\gamma_1, \gamma_2). \tag{26}$$
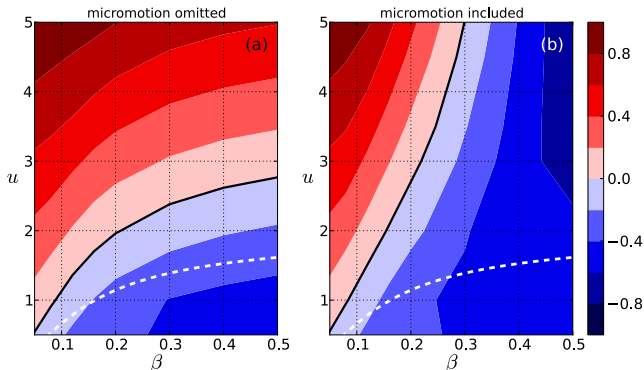

FIG. 4. The phase diagram showing the manybody gap Δ as a function of the inverse shaking frequency β and the dimensionless interaction strength u for eight-boson system. Micromotion-induced interactions are omitted in panel (a) and taken into account to the third order in panel (b). The full black lines delimit the regions of positive manybody gaps (shown in red shades) and differ considerably between the panels. The white dashed line indicates the parameter regime where the interaction strength U is equal to the single-particle bandgap. Well below this line mixing between single-particle bands becomes small.
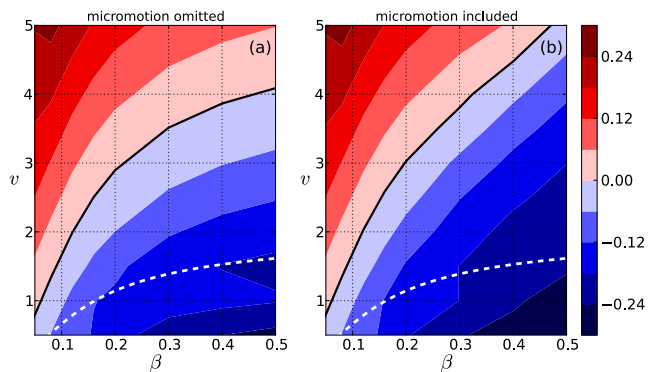

FIG. 5. The same as Fig. 4 but for eight-fermion system with dimensionless NN repulsion energy v. Note that the scale of the colorbar, and correspondingly the typical manybody gaps are significantly smaller than for bosons.

The complete phase diagrams in the β-u (resp. β-v) plane for bosons (resp. fermions) occupying the lower (resp. upper) single-particle band at $1/3$ (resp. $1/2$) filling are shown in Figs. 4 and 5. In both instances we map out the behavior of the manybody gap as a function of the governing parameters, β and u (resp. v). The red areas correspond to the presence of a positive manybody gap implying that the states comprising the GSM are isolated from the remaining ones *everywhere* in the MBZ and thus the two manifolds do not mix. On the contrary, blue areas correspond to a *negative* manybody gap. In this situation, at least one state from the GSM attains higher energy value than the lowest state not belonging to the GSM, and the two manifolds overlap somewhere in the MBZ. The full black line separates phase space areas characterized by manybody gaps of different signs and thus serves as a first criterion for the possibility of formation of the Floquet fractional Chern insulator. Of course, this criterion takes into account only the aspects of the energy spectra and must be further supported by, e. g., information obtained from excitation spectra discussed in the following subsection. Nevertheless, already these phase diagrams indicate that inclusion of micromotion-induced interactions typically pushes the phase boundary upwards in the phase diagram. That is, stronger interactions will be needed to stabilize FCI phases at equal other conditions.

Bosonic lattice systems seem to be much more promising candidates for the stabilization of FCI phases than fermionic ones. Indeed, they find a realization in quantum gas experiments where strong and tunable onsite interactions are possible, and Fig. 4 reveals that in bosonic systems large manybody gaps on the order of the tunneling amplitude J can be obtained. In contrast, for fermionic systems nearest-neighbor repulsions are harder to tune into strongly-interacting limit (in graphene the strength of NN repulsion is estimated[77] to be around $2J$), and the overall scale of attainable manybody gaps is also smaller, as demonstrated by Fig. 5.

Viewing FCI states as direct analogues of Laughlin's fractional quantum Hall states, one would ideally prefer working in the regime where the fractional states are induced by strong interactions mixing single-particle states within a single topological (Chern or Landau) band and not among several bands. (Recent results suggest, however, that weak interband mixing is not detrimental for the formation of fermionic $\nu = \frac{1}{3}$ FCI state[78,79]). This corresponds to the situation where the single-particle bandgap exceeds the characteristic interaction strength. In Figs. 4 and 5, the white dashed lines indicate the regime where the corresponding interaction parameter, U or V, is equal to the single-particle bandgap; well below these lines mixing between single-particle bands is small. Obviously, the approximation based on the band projection is not justified in the considered regime. Moreover, the interaction strengths required to stabilize FCI phases in the current model also generally exceed the above-stated limit. These observations suggest that it must be quite challenging to explore FCI phases within the considered model. A window of opportunity might persist at the higher end of the considered range of driving frequencies (equivalently, at the lower end of the range of β's). Although the approximation focusing on just one single-particle band is not fully justified here, the effects of band mixing were reported not to be critical.[78,79] In this limit, notably weaker interaction strengths are required to stabilize FCI phases [see Figs. 4 and 5], and moreover, problems caused by heating due to the resonant excitation of collective excitations become smaller.
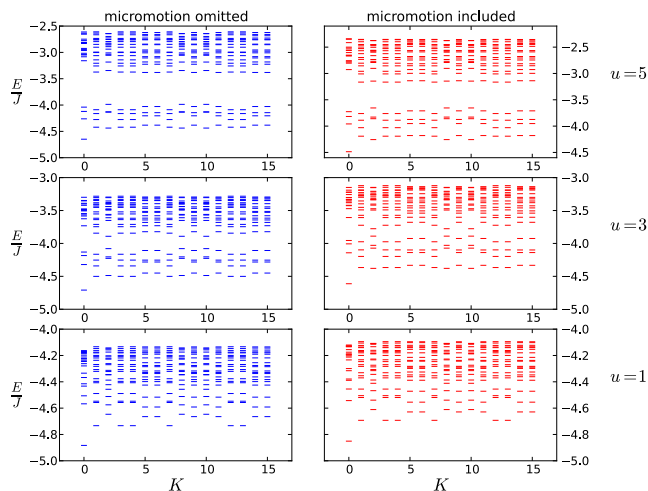
C. Quasihole spectra

FIG. 6. Quasihole excitation spectra for eight-boson system calculated at the inverse dimensionless driving strength $\beta = 0.1$. Formation of an isolated manifold of 4×16 states is visible for strong interactions with $u = 5$, and gradually closes when interaction become weaker.

Finally, let us also take a brief look at the quasihole excitation spectra, corresponding to the removal of a particle from the ground state.[12] Here, we are driven by twofold motivation. On the one hand, these spectra serve as an additional identification check confirming that the obtained phases display behavior characteristic of fractional Chern insulator. Thus, one expects to observe the formation of an isolated low-energy manifold of quasihole states whose number is predicted by counting rules based on the generalized Pauli principle.[12] On the other hand, one is interested in the the evolution of the size of the gap separating the low-energy manifold from the remaining states as a function of the computational parameters. In this way, we also obtain complementary information about the interaction strengths that are sufficient to induce the FCI phases.

Qualitatively similar results are obtained for both fermionic and bosonic systems. Focusing on the latter, we perform exact diagonalizations for systems of 7 bosonic particles moving on a lattice consisting of 4×4 elementary cells. This is one particle less than would correspond to the exact $1/2$ filling of the band, and can be interpreted as an introduction of a hole into the previously studied system. In this specific case, the $(1, 2)$-admissible counting rule[12] predicts the formation of an isolated manifold with 4 states per each total quasimomentum sector, implying the total of 64 states. The actual numerical results obtained for $\beta = 0.1$ and varying values of the interaction strength are shown in Fig. 6. In all panels, the abscissa axes enumerate the total quasimomentum sectors indexed by the integer values K running from zero to $15 \equiv 4 \times 4 - 1$, and the ordinate axes display the energies of the lowest manybody states obtained from the exact-diagonalization calculations. The left (resp. right) column of three plots corresponds to omitted (resp. included to the third order) micromotion-induced corrections to the effective Hamiltonian. The strength of particle interactions $u = U/J$ is decreasing from the top to the bottom. At the strongest considered interactions, $u = 5$ (top row) one sees a clear gap separating the lower group of exactly four states per quasimomentum sector from the rest of the spectrum. For weaker interactions ($u = 3$ in the middle row) the gap is barely discernible in the absence of micromotion-induced interactions and is obliterated when micromotion is taken into account. Finally, the in bottom row corresponding to weak interactions with $u = 1$ there is no visible gap indicating the absence of FCI phase. In general, the information provided by the quasihole spectra is broadly compatible with that obtained from the ordinary manybody spectra, however, the constraints placed on interactions being "sufficiently strong" are even more stringent, thus further contributing to the pessimistic outlook on the feasibility of fractional Chern insulating states in the studied system.

IV. CONCLUSIONS

To summarize, we address the issue of the stabilization of Floquet fractional Chern insulator states for strongly interacting particles (bosons or fermions) on a time-periodically driven honeycomb lattice. In this system, the necessary topological single particle bands are formed due to the next-nearest neighbor transitions, which is a second-order effect corresponding to two consecutive tunneling events during a single driving period. This requires sufficiently low driving frequencies and necessitates the consideration of further expansion terms beyond the averaging of the Hamiltonian used in high-frequency schemes. The third-order terms describe the coupling of real-space micromotion and interactions. In strongly interacting systems, the importance of these terms is, in general, comparable to that of the second-order contributions. The prefactor features not only the expansion parameter $(\hbar\omega)^{-1}$ but also the onsite repulsion energy U for bosonic systems or, alternatively, nearest-site repulsion energy V for fermionic systems. Within simulations of small systems, the coupling of micromotion and interactions turns out to be both significant and detrimental to the formation of quantum-Hall like states. Thus, the realization of Floquet fractional Chern insulator states seems rather challenging.

Appendix A: Haldane model

The Haldane model[1,28,34,39,80–84] sets a paradigmatic example of the topological bandstructure supported by a simple two-band setup. This model features a honeycomb lattice (see Fig. 1) with nearest-neighbor hopping described by a real amplitude $-J_1$ plus next-nearest neighbor hopping described by a *complex* amplitude $-J_2\,e^{i\varphi}$ (resp. $-J_2\,e^{-i\varphi}$) in the counter-clockwise (resp. clockwise) direction. In the quasimomentum representation, the Hamiltonian matrix reads

$$H(\boldsymbol{k}) = \begin{bmatrix} -J_2\tilde{f}(\boldsymbol{k},\varphi) & -J_1 g^*(\boldsymbol{k}) \\ -J_1 g(\boldsymbol{k}) & -J_2\tilde{f}(\boldsymbol{k},-\varphi) \end{bmatrix}, \qquad \text{(A1)}$$

with

$$g(\boldsymbol{k}) = \sum_{j=1}^{3} e^{-i\boldsymbol{k}\cdot(\boldsymbol{\delta}_j-\boldsymbol{\delta}_1)} = 1 + e^{i(k_1+k_2)} + e^{ik_2}, \quad \text{(A2)}$$

$$\begin{aligned} \tilde{f}(\boldsymbol{k},\varphi) &= 2\sum_{j=1}^{3}\cos\left(\boldsymbol{k}\cdot\boldsymbol{a}_j - \varphi\right) \\ &= 2\left[\cos(k_1-\varphi) + \cos(k_2-\varphi)\right. \\ &\quad \left. + \cos(k_1+k_2+\varphi)\right]. \end{aligned} \qquad \text{(A3)}$$

Here we define $\boldsymbol{k} = (k_1/2\pi)\,\boldsymbol{b}_1 + (k_2/2\pi)\,\boldsymbol{b}_2$, with $\boldsymbol{b}_{1,2}$ denoting the reciprocal lattice vectors, and $(k_1,k_2) \in [0,2\pi) \times [0,2\pi)$ covering the rhombic Brillouin zone. In the case considered in the main text, the NNN hopping amplitude is purely imaginary, corresponding to $\varphi \to \pi/2$, and therefore

$$H(\boldsymbol{k}) = \begin{bmatrix} -J_2 f(\boldsymbol{k}) & -J_1 g^*(\boldsymbol{k}) \\ -J_1 g(\boldsymbol{k}) & J_2 f(\boldsymbol{k}) \end{bmatrix}, \qquad \text{(A4)}$$

with the unchanged definition for $g(\boldsymbol{k})$, and

$$f(\boldsymbol{k}) = 2\left[\sin k_1 + \sin k_2 - \sin(k_1+k_2)\right]. \qquad \text{(A5)}$$

While the resulting bands are not globally flat, they feature flat sections that cover BZ regions characterized by large Berry curvatures. This fact forms the basis for the anticipation[17] that the Haldane model might support FCI phases for strongly interacting particles.
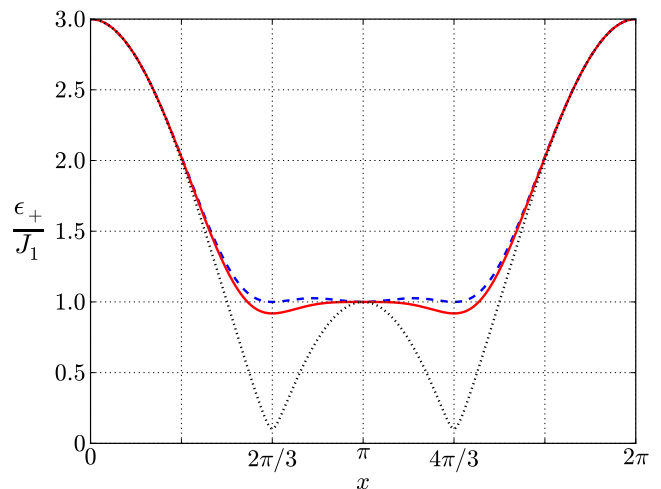
FIG. 7. Dispersion of the upper band of the Haldane model drawn along the diagonal of the rhombic BZ.

The formation of the flat segments in the energy bands is best visualized focusing on a one-dimensional cut through the rhombic BZ along its diagonal (obtained by setting $k_1 = k_2$). This line connects the zone center at $(0,0)$ to the equivalent point at $(2\pi,2\pi)$, and passes through both inequivalent Dirac points at $(2\pi/3, 2\pi/3)$

and $(4\pi/3, 4\pi/3)$. Using the single coordinate, $x \equiv k_1 = k_2$, we simplify (A2) and (A5) to read

$$g(x) = 1 + e^{ix} + e^{i2x}, \qquad (A6)$$

$$f(x) = 4\sin x - 2\sin 2x, \qquad (A7)$$

and obtain the scaled band energies

$$\frac{\epsilon_\pm}{J_1} = \pm \left[\left(\frac{J_2}{J_1}\right)^2 f^2(x) + |g(x)|^2 \right]^{1/2}. \qquad (A8)$$

The two bands are mirror-symmetric with respect to the line $\epsilon = 0$, and the dispersion of the upper band is shown in Fig. 7 for a few selected values of the governing parameter $F = J_2/J_1$. Weak NNN hopping amplitudes open small topological gaps at the Dirac points, as illustrated by the dotted black line corresponding to $F = 0.02$. Stronger couplings produce relatively dispersionless portions of the bands. In Fig. 7, this result is illustrated by the full red and dashed blue lines drawn, respectively for $F_Q = 1/\sqrt{32}$ and $F_D = 1/\sqrt{27}$. The two reference values are obtained from different flatness criteria, and are very similar. The first value, F_Q, is defined by the requirement that the Taylor expansion of the energy ϵ_+/J around the midpoint $x = \pi$ starts with the quartic (rather than the second order) term. The latter value, F_D, is the smallest at which the bandgap at the Dirac points becomes equal to the gap at the midpoint of the BZ diagonal. These two alternative criteria lead only to miniscule variations in the resulting manybody bandstructure, and we choose to adopt the value F_Q as the reference.

Appendix B: Operators in quasimomentum representation

In the main text, we discuss the constituent parts of the effective Hamiltonian using their real-space forms which typically lend themselves to physically transparent interpretation as combinations of hopping and interaction events. The purpose of the present Appendix is to give the corresponding expressions in the reciprocal space, used in the actual numerical work.

Denoting the number of elementary cells in the lattice N_s, we define the reciprocal-space creation operators $\hat{a}_{\boldsymbol{k}A}^\dagger$ and $\hat{a}_{\boldsymbol{k}B}^\dagger$ in terms of the usual Fourier transforms

$$\hat{a}_{\boldsymbol{k}A}^\dagger = \frac{1}{\sqrt{N_s}} \sum_{i \in A} \hat{a}_i^\dagger \, e^{i\boldsymbol{k}\cdot\boldsymbol{r}_i}, \qquad (B1)$$

$$\hat{a}_{\boldsymbol{k}B}^\dagger = \frac{1}{\sqrt{N_s}} \sum_{i \in B} \hat{a}_i^\dagger \, e^{i\boldsymbol{k}\cdot(\boldsymbol{r}_i - \boldsymbol{\delta}_1)}, \qquad (B2)$$

with the conjugate version of this equation applicable to annihilation operators. Note that in the quasimomentum representation we explicitly specify the sublattice index A or B while in the real space this was avoided by using the shorthand notation i versus $i + \mu$.

The first-order contribution to the effective Hamiltonian is now written

$$\hat{H}_F^{(1)} = \hat{H}_{\text{int}} - J\mathcal{J}_0(\alpha) \sum_{\boldsymbol{k}} \left[\hat{a}_{\boldsymbol{k}B}^\dagger \hat{a}_{\boldsymbol{k}A} \, g(\boldsymbol{k}) + h.c. \right], \quad (B3)$$

with $g(\boldsymbol{k}) = \sum_\mu e^{-i\boldsymbol{k}\cdot(\boldsymbol{\delta}_\mu - \boldsymbol{\delta}_1)}$. The interaction Hamiltonian reads for bosons

$$\hat{H}_{\text{int}}^{(b)} = \frac{1}{2} \sum_{\{\boldsymbol{k}\}} W_b\left(\{\boldsymbol{k}\}\right) \Big[\hat{a}_{\boldsymbol{k}_1 A}^\dagger \hat{a}_{\boldsymbol{k}_2 A}^\dagger \hat{a}_{\boldsymbol{k}_3 A} \hat{a}_{\boldsymbol{k}_4 A}$$
$$+ \hat{a}_{\boldsymbol{k}_1 B}^\dagger \hat{a}_{\boldsymbol{k}_2 B}^\dagger \hat{a}_{\boldsymbol{k}_3 B} \hat{a}_{\boldsymbol{k}_4 B} \Big], \qquad (B4a)$$

$$W_b\left(\{\boldsymbol{k}\}\right) = \frac{U}{N_s} \delta'_{\boldsymbol{k}_1 + \boldsymbol{k}_2, \boldsymbol{k}_3 + \boldsymbol{k}_4}, \qquad (B4b)$$

and for fermions

$$\hat{H}_{\text{int}}^{(f)} = \sum_{\{\boldsymbol{k}\}} \hat{a}_{\boldsymbol{k}_1 B}^\dagger \hat{a}_{\boldsymbol{k}_2 A}^\dagger \hat{a}_{\boldsymbol{k}_3 A} \hat{a}_{\boldsymbol{k}_4 B} \cdot W_f\left(\{\boldsymbol{k}\}\right), \quad (B5a)$$

$$W_f\left(\{\boldsymbol{k}\}\right) = \frac{V}{N_s} g(\boldsymbol{k}_1 - \boldsymbol{k}_4) \, \delta'_{\boldsymbol{k}_1 + \boldsymbol{k}_2, \boldsymbol{k}_3 + \boldsymbol{k}_4}, \quad (B5b)$$

with the periodic Kronecker delta that allows the quasi-momenta in its arguments to differ by an elementary translation on the reciprocal lattice. The symbol $\{\boldsymbol{k}\} \equiv (\boldsymbol{k}_1, \boldsymbol{k}_2, \boldsymbol{k}_3, \boldsymbol{k}_4)$ stands for the set of four quasimomenta involved in a scattering event.

Proceeding to the second order we write

$$\hat{H}_1 = -J\mathcal{J}_1(\alpha) \sum_{\boldsymbol{k}} \left[\hat{a}_{\boldsymbol{k}B}^\dagger \hat{a}_{\boldsymbol{k}A} h_{BA}(\boldsymbol{k}) + \hat{a}_{\boldsymbol{k}A}^\dagger \hat{a}_{\boldsymbol{k}B} h_{AB}(\boldsymbol{k}), \right]$$
$$(B6)$$

with

$$h_{BA}(\boldsymbol{k}) = \sum_{\mu=1}^{3} e^{-i\boldsymbol{k}\cdot(\boldsymbol{\delta}_\mu - \boldsymbol{\delta}_1)} e^{-i\varphi_\mu}, \qquad (B7a)$$

$$h_{AB}(\boldsymbol{k}) = -\sum_{\mu=1}^{3} e^{i\boldsymbol{k}\cdot(\boldsymbol{\delta}_\mu - \boldsymbol{\delta}_1)} e^{-i\varphi_\mu}, \qquad (B7b)$$

and evaluating the commutator in Eq. (18b) obtain

$$\hat{H}_F^{(2)} = \frac{1}{\hbar\omega} \left[\hat{H}_1, \hat{H}_1^\dagger \right] = \frac{\sqrt{3}J^2 \mathcal{J}_1^2(\alpha)}{\hbar\omega}$$
$$\times \sum_{\boldsymbol{k}} f(\boldsymbol{k}) \left[\hat{a}_{\boldsymbol{k}A}^\dagger \hat{a}_{\boldsymbol{k}A} - \hat{a}_{\boldsymbol{k}B}^\dagger \hat{a}_{\boldsymbol{k}B} \right], \qquad (B8)$$

with $f(\boldsymbol{k}) = 2\sum_j \sin \boldsymbol{k} \cdot \boldsymbol{a}_j$. These terms are diagonal and describe NNN hopping on separate sublattices.

To describe the coupling of micromotion and interactions, we evaluate the nested commutators in Eq. (18c) and obtain, depending on the statistics,

$$\hat{H}_F^{(3,b|f)} = -\frac{J^2 \mathcal{J}_1^2(\alpha)}{2(\hbar\omega)^2} \sum_{\{\boldsymbol{k}\}} W_{b|f}(\{\boldsymbol{k}\}) \, \mathcal{S}_{b|f}, \qquad (B9)$$

with

$$\mathcal{S}_{\mathrm{b}}(\{\boldsymbol{k}\}) = + h_{\mathrm{AB}}(\boldsymbol{k}_3)\,h_{\mathrm{AB}}^*(\boldsymbol{k}_3)\,\hat{a}_{\boldsymbol{k}_1\mathrm{A}}^\dagger\hat{a}_{\boldsymbol{k}_2\mathrm{A}}^\dagger\hat{a}_{\boldsymbol{k}_3\mathrm{A}}\hat{a}_{\boldsymbol{k}_4\mathrm{A}} - h_{\mathrm{AB}}(\boldsymbol{k}_3)\,h_{\mathrm{AB}}^*(\boldsymbol{k}_1)\,\hat{a}_{\boldsymbol{k}_1\mathrm{B}}^\dagger\hat{a}_{\boldsymbol{k}_2\mathrm{A}}^\dagger\hat{a}_{\boldsymbol{k}_3\mathrm{B}}\hat{a}_{\boldsymbol{k}_4\mathrm{A}}$$

$$- h_{\mathrm{AB}}(\boldsymbol{k}_3)\,h_{\mathrm{AB}}^*(\boldsymbol{k}_2)\,\hat{a}_{\boldsymbol{k}_1\mathrm{A}}^\dagger\hat{a}_{\boldsymbol{k}_2\mathrm{B}}^\dagger\hat{a}_{\boldsymbol{k}_3\mathrm{B}}\hat{a}_{\boldsymbol{k}_4\mathrm{A}} + h_{\mathrm{AB}}(\boldsymbol{k}_3)\,h_{\mathrm{BA}}^*(\boldsymbol{k}_4)\,\hat{a}_{\boldsymbol{k}_1\mathrm{A}}^\dagger\hat{a}_{\boldsymbol{k}_2\mathrm{A}}^\dagger\hat{a}_{\boldsymbol{k}_3\mathrm{B}}\hat{a}_{\boldsymbol{k}_4\mathrm{B}}$$

$$+ h_{\mathrm{AB}}(\boldsymbol{k}_4)\,h_{\mathrm{AB}}^*(\boldsymbol{k}_4)\,\hat{a}_{\boldsymbol{k}_1\mathrm{A}}^\dagger\hat{a}_{\boldsymbol{k}_2\mathrm{A}}^\dagger\hat{a}_{\boldsymbol{k}_3\mathrm{A}}\hat{a}_{\boldsymbol{k}_4\mathrm{A}} - h_{\mathrm{AB}}(\boldsymbol{k}_4)\,h_{\mathrm{AB}}^*(\boldsymbol{k}_1)\,\hat{a}_{\boldsymbol{k}_1\mathrm{B}}^\dagger\hat{a}_{\boldsymbol{k}_2\mathrm{A}}^\dagger\hat{a}_{\boldsymbol{k}_3\mathrm{A}}\hat{a}_{\boldsymbol{k}_4\mathrm{B}}$$

$$- h_{\mathrm{AB}}(\boldsymbol{k}_4)\,h_{\mathrm{AB}}^*(\boldsymbol{k}_2)\,\hat{a}_{\boldsymbol{k}_1\mathrm{A}}^\dagger\hat{a}_{\boldsymbol{k}_2\mathrm{B}}^\dagger\hat{a}_{\boldsymbol{k}_3\mathrm{A}}\hat{a}_{\boldsymbol{k}_4\mathrm{B}} + h_{\mathrm{AB}}(\boldsymbol{k}_4)\,h_{\mathrm{BA}}^*(\boldsymbol{k}_3)\,\hat{a}_{\boldsymbol{k}_1\mathrm{A}}^\dagger\hat{a}_{\boldsymbol{k}_2\mathrm{A}}^\dagger\hat{a}_{\boldsymbol{k}_3\mathrm{B}}\hat{a}_{\boldsymbol{k}_4\mathrm{B}}$$

$$+ h_{\mathrm{BA}}(\boldsymbol{k}_1)\,h_{\mathrm{AB}}^*(\boldsymbol{k}_2)\,\hat{a}_{\boldsymbol{k}_1\mathrm{B}}^\dagger\hat{a}_{\boldsymbol{k}_2\mathrm{B}}^\dagger\hat{a}_{\boldsymbol{k}_3\mathrm{A}}\hat{a}_{\boldsymbol{k}_4\mathrm{A}} - h_{\mathrm{BA}}(\boldsymbol{k}_1)\,h_{\mathrm{BA}}^*(\boldsymbol{k}_3)\,\hat{a}_{\boldsymbol{k}_1\mathrm{B}}^\dagger\hat{a}_{\boldsymbol{k}_2\mathrm{A}}^\dagger\hat{a}_{\boldsymbol{k}_3\mathrm{B}}\hat{a}_{\boldsymbol{k}_4\mathrm{A}} \qquad (\mathrm{B10})$$

$$- h_{\mathrm{BA}}(\boldsymbol{k}_1)\,h_{\mathrm{BA}}^*(\boldsymbol{k}_4)\,\hat{a}_{\boldsymbol{k}_1\mathrm{B}}^\dagger\hat{a}_{\boldsymbol{k}_2\mathrm{A}}^\dagger\hat{a}_{\boldsymbol{k}_3\mathrm{A}}\hat{a}_{\boldsymbol{k}_4\mathrm{B}} + h_{\mathrm{BA}}(\boldsymbol{k}_1)\,h_{\mathrm{BA}}^*(\boldsymbol{k}_1)\,\hat{a}_{\boldsymbol{k}_1\mathrm{A}}^\dagger\hat{a}_{\boldsymbol{k}_2\mathrm{A}}^\dagger\hat{a}_{\boldsymbol{k}_3\mathrm{A}}\hat{a}_{\boldsymbol{k}_4\mathrm{A}}$$

$$+ h_{\mathrm{BA}}(\boldsymbol{k}_2)\,h_{\mathrm{AB}}^*(\boldsymbol{k}_1)\,\hat{a}_{\boldsymbol{k}_1\mathrm{B}}^\dagger\hat{a}_{\boldsymbol{k}_2\mathrm{B}}^\dagger\hat{a}_{\boldsymbol{k}_3\mathrm{A}}\hat{a}_{\boldsymbol{k}_4\mathrm{A}} - h_{\mathrm{BA}}(\boldsymbol{k}_2)\,h_{\mathrm{BA}}^*(\boldsymbol{k}_3)\,\hat{a}_{\boldsymbol{k}_1\mathrm{A}}^\dagger\hat{a}_{\boldsymbol{k}_2\mathrm{B}}^\dagger\hat{a}_{\boldsymbol{k}_3\mathrm{B}}\hat{a}_{\boldsymbol{k}_4\mathrm{A}}$$

$$- h_{\mathrm{BA}}(\boldsymbol{k}_2)\,h_{\mathrm{BA}}^*(\boldsymbol{k}_4)\,\hat{a}_{\boldsymbol{k}_1\mathrm{A}}^\dagger\hat{a}_{\boldsymbol{k}_2\mathrm{B}}^\dagger\hat{a}_{\boldsymbol{k}_3\mathrm{A}}\hat{a}_{\boldsymbol{k}_4\mathrm{B}} + h_{\mathrm{BA}}(\boldsymbol{k}_2)\,h_{\mathrm{BA}}^*(\boldsymbol{k}_2)\,\hat{a}_{\boldsymbol{k}_1\mathrm{A}}^\dagger\hat{a}_{\boldsymbol{k}_2\mathrm{A}}^\dagger\hat{a}_{\boldsymbol{k}_3\mathrm{A}}\hat{a}_{\boldsymbol{k}_4\mathrm{A}},$$

$$+ h.c. + \Big\{ \mathrm{A} \leftrightarrow \mathrm{B} \Big\},$$

$$\mathcal{S}_{\mathrm{f}}(\{\boldsymbol{k}\}) = - h_{\mathrm{BA}}(\boldsymbol{k}_4)\,h_{\mathrm{AB}}^*(\boldsymbol{k}_2)\,\hat{a}_{\boldsymbol{k}_1\mathrm{B}}^\dagger\hat{a}_{\boldsymbol{k}_2\mathrm{B}}^\dagger\hat{a}_{\boldsymbol{k}_3\mathrm{A}}\hat{a}_{\boldsymbol{k}_4\mathrm{A}} - h_{\mathrm{BA}}(\boldsymbol{k}_2)\,h_{\mathrm{AB}}^*(\boldsymbol{k}_4)\,\hat{a}_{\boldsymbol{k}_1\mathrm{B}}^\dagger\hat{a}_{\boldsymbol{k}_2\mathrm{B}}^\dagger\hat{a}_{\boldsymbol{k}_3\mathrm{A}}\hat{a}_{\boldsymbol{k}_4\mathrm{A}}$$

$$- h_{\mathrm{BA}}(\boldsymbol{k}_4)\,h_{\mathrm{BA}}^*(\boldsymbol{k}_1)\,\hat{a}_{\boldsymbol{k}_1\mathrm{A}}^\dagger\hat{a}_{\boldsymbol{k}_2\mathrm{A}}^\dagger\hat{a}_{\boldsymbol{k}_3\mathrm{A}}\hat{a}_{\boldsymbol{k}_4\mathrm{A}} + h_{\mathrm{BA}}(\boldsymbol{k}_4)\,h_{\mathrm{BA}}^*(\boldsymbol{k}_3)\,\hat{a}_{\boldsymbol{k}_1\mathrm{B}}^\dagger\hat{a}_{\boldsymbol{k}_2\mathrm{A}}^\dagger\hat{a}_{\boldsymbol{k}_3\mathrm{B}}\hat{a}_{\boldsymbol{k}_4\mathrm{A}}$$

$$+ h_{\mathrm{BA}}(\boldsymbol{k}_4)\,h_{\mathrm{BA}}^*(\boldsymbol{k}_4)\,\hat{a}_{\boldsymbol{k}_1\mathrm{B}}^\dagger\hat{a}_{\boldsymbol{k}_2\mathrm{A}}^\dagger\hat{a}_{\boldsymbol{k}_3\mathrm{A}}\hat{a}_{\boldsymbol{k}_4\mathrm{B}} + h_{\mathrm{BA}}(\boldsymbol{k}_2)\,h_{\mathrm{BA}}^*(\boldsymbol{k}_1)\,\hat{a}_{\boldsymbol{k}_1\mathrm{A}}^\dagger\hat{a}_{\boldsymbol{k}_2\mathrm{B}}^\dagger\hat{a}_{\boldsymbol{k}_3\mathrm{A}}\hat{a}_{\boldsymbol{k}_4\mathrm{B}}$$

$$+ h_{\mathrm{BA}}(\boldsymbol{k}_2)\,h_{\mathrm{BA}}^*(\boldsymbol{k}_2)\,\hat{a}_{\boldsymbol{k}_1\mathrm{B}}^\dagger\hat{a}_{\boldsymbol{k}_2\mathrm{A}}^\dagger\hat{a}_{\boldsymbol{k}_3\mathrm{A}}\hat{a}_{\boldsymbol{k}_4\mathrm{B}} - h_{\mathrm{BA}}(\boldsymbol{k}_2)\,h_{\mathrm{BA}}^*(\boldsymbol{k}_3)\,\hat{a}_{\boldsymbol{k}_1\mathrm{B}}^\dagger\hat{a}_{\boldsymbol{k}_2\mathrm{B}}^\dagger\hat{a}_{\boldsymbol{k}_3\mathrm{B}}\hat{a}_{\boldsymbol{k}_4\mathrm{B}}$$

$$- h_{\mathrm{AB}}(\boldsymbol{k}_3)\,h_{\mathrm{AB}}^*(\boldsymbol{k}_2)\,\hat{a}_{\boldsymbol{k}_1\mathrm{B}}^\dagger\hat{a}_{\boldsymbol{k}_2\mathrm{B}}^\dagger\hat{a}_{\boldsymbol{k}_3\mathrm{B}}\hat{a}_{\boldsymbol{k}_4\mathrm{B}} + h_{\mathrm{AB}}(\boldsymbol{k}_3)\,h_{\mathrm{AB}}^*(\boldsymbol{k}_3)\,\hat{a}_{\boldsymbol{k}_1\mathrm{B}}^\dagger\hat{a}_{\boldsymbol{k}_2\mathrm{A}}^\dagger\hat{a}_{\boldsymbol{k}_3\mathrm{A}}\hat{a}_{\boldsymbol{k}_4\mathrm{B}} \qquad (\mathrm{B11})$$

$$+ h_{\mathrm{AB}}(\boldsymbol{k}_3)\,h_{\mathrm{AB}}^*(\boldsymbol{k}_4)\,\hat{a}_{\boldsymbol{k}_1\mathrm{B}}^\dagger\hat{a}_{\boldsymbol{k}_2\mathrm{A}}^\dagger\hat{a}_{\boldsymbol{k}_3\mathrm{B}}\hat{a}_{\boldsymbol{k}_4\mathrm{A}} + h_{\mathrm{AB}}(\boldsymbol{k}_1)\,h_{\mathrm{AB}}^*(\boldsymbol{k}_1)\,\hat{a}_{\boldsymbol{k}_1\mathrm{B}}^\dagger\hat{a}_{\boldsymbol{k}_2\mathrm{A}}^\dagger\hat{a}_{\boldsymbol{k}_3\mathrm{A}}\hat{a}_{\boldsymbol{k}_4\mathrm{B}}$$

$$+ h_{\mathrm{AB}}(\boldsymbol{k}_1)\,h_{\mathrm{AB}}^*(\boldsymbol{k}_2)\,\hat{a}_{\boldsymbol{k}_1\mathrm{A}}^\dagger\hat{a}_{\boldsymbol{k}_2\mathrm{B}}^\dagger\hat{a}_{\boldsymbol{k}_3\mathrm{A}}\hat{a}_{\boldsymbol{k}_4\mathrm{B}} - h_{\mathrm{AB}}(\boldsymbol{k}_1)\,h_{\mathrm{AB}}^*(\boldsymbol{k}_4)\,\hat{a}_{\boldsymbol{k}_1\mathrm{A}}^\dagger\hat{a}_{\boldsymbol{k}_2\mathrm{A}}^\dagger\hat{a}_{\boldsymbol{k}_3\mathrm{A}}\hat{a}_{\boldsymbol{k}_4\mathrm{A}}$$

$$- h_{\mathrm{AB}}(\boldsymbol{k}_3)\,h_{\mathrm{BA}}^*(\boldsymbol{k}_1)\,\hat{a}_{\boldsymbol{k}_1\mathrm{A}}^\dagger\hat{a}_{\boldsymbol{k}_2\mathrm{A}}^\dagger\hat{a}_{\boldsymbol{k}_3\mathrm{B}}\hat{a}_{\boldsymbol{k}_4\mathrm{B}} - h_{\mathrm{AB}}(\boldsymbol{k}_1)\,h_{\mathrm{BA}}^*(\boldsymbol{k}_3)\,\hat{a}_{\boldsymbol{k}_1\mathrm{A}}^\dagger\hat{a}_{\boldsymbol{k}_2\mathrm{A}}^\dagger\hat{a}_{\boldsymbol{k}_3\mathrm{B}}\hat{a}_{\boldsymbol{k}_4\mathrm{B}}$$

$$+ h.c..$$

* egidijus.anisimovas@ff.vu.lt

† eckardt@pks.mpg.de

[1] F. D. M. Haldane, Phys. Rev. Lett. **61**, 2015 (1988).

[2] M. Z. Hasan and C. L. Kane, Rev. Mod. Phys. **82**, 3045 (2010).

[3] X.-L. Qi and S.-C. Zhang, Rev. Mod. Phys. **83**, 1057 (2011).

[4] B. A. Bernevig, T. L. Hughes, and S.-C. Zhang, Science **314**, 1757 (2006).

[5] D. Hsieh, D. Qian, L. Wray, Y. Xia, Y. S. Hor, R. J. Cava, and M. Z. Hasan, Nature **452**, 970 (2008).

[6] M. König, S. Wiedmann, C. Brüne, A. Roth, H. Buhmann, L. W. Molenkamp, X.-L. Qi, and S.-C. Zhang, Science **318**, 766 (2007).

[7] C. L. Kane and E. J. Mele, Phys. Rev. Lett. **95**, 146802 (2005).

[8] C. L. Kane and E. J. Mele, Phys. Rev. Lett. **95**, 226801 (2005).

[9] K. von Klitzing, Rev. Mod. Phys. **58**, 519 (1986).

[10] D. N. Sheng, Z.-C. Gu, K. Sun, and L. Sheng, Nat. Commun. **2**, 389 (2011).

[11] T. Neupert, L. Santos, C. Chamon, and C. Mudry, Phys. Rev. Lett. **106**, 236804 (2011).

[12] N. Regnault and B. A. Bernevig, Phys. Rev. X **1**, 021014 (2011).

[13] Y.-F. Wang, Z.-C. Gu, C.-D. Gong, and D. N. Sheng, Phys. Rev. Lett. **107**, 146803 (2011).

[14] Y.-L. Wu, B. A. Bernevig, and N. Regnault, Phys. Rev. B **85**, 075116 (2012).

[15] E. J. Bergholtz and Z. Liu, Int. J. Mod. Phys. B **27**, 1330017 (2013).

[16] S. A. Parameswaran, R. Roy, and S. L. Sondhi, C. R. Phys. **14**, 816 (2013).

[17] A. G. Grushin, Á. Gómez-León, and T. Neupert, Phys. Rev. Lett. **112**, 156801 (2014).

[18] A. Eckardt, C. Weiss, and M. Holthaus, Phys. Rev. Lett. **95**, 260404 (2005).

[19] H. Lignier, C. Sias, D. Ciampini, Y. Singh, A. Zenesini, O. Morsch, and E. Arimondo, Phys. Rev. Lett. **99**, 220403 (2007).

[20] C. Sias, H. Lignier, Y. P. Singh, A. Zenesini, D. Ciampini, O. Morsch, and E. Arimondo, Phys. Rev. Lett. **100**, 040404 (2008).

[21] A. Zenesini, H. Lignier, D. Ciampini, O. Morsch, and E. Arimondo, Phys. Rev. Lett. **102**, 100403 (2009).

[22] A. Alberti, V. V. Ivanov, G. M. Tino, and G. Ferrari, Nat. Phys. **5**, 547 (2009).

[23] A. Eckardt, P. Hauke, P. Soltan-Panahi, C. Becker, K. Sengstock, and M. Lewenstein, Europhys. Lett. **89**, 10010 (2010).

[24] E. Haller, R. Hart, M. J. Mark, J. G. Danzl, L. Reichsöllner, and H.-C. Nägerl, Phys. Rev. Lett. **104**, 200403 (2010).

[25] J. Struck, C. Ölschläger, R. Le Targat, P. Soltan-Panahi,

A. Eckardt, M. Lewenstein, P. Windpassinger, and K. Sengstock, Science **333**, 996 (2011).

[26] A. R. Kolovsky, Europhys. Lett. **93**, 20003 (2011).

[27] M. Aidelsburger, M. Atala, S. Nascimbène, S. Trotzky, Y.-A. Chen, and I. Bloch, Phys. Rev. Lett. **107**, 255301 (2011).

[28] P. Hauke, O. Tieleman, A. Celi, C. Ölschläger, J. Simonet, J. Struck, M. Weinberg, P. Windpassinger, K. Sengstock, M. Lewenstein, and A. Eckardt, Phys. Rev. Lett. **109**, 145301 (2012).

[29] J. Struck, C. Ölschläger, M. Weinberg, P. Hauke, J. Simonet, A. Eckardt, M. Lewenstein, K. Sengstock, and P. Windpassinger, Phys. Rev. Lett. **108**, 225304 (2012).

[30] J. Struck, M. Weinberg, C. Ölschläger, P. Windpassinger, J. Simonet, K. Sengstock, R. Höppner, P. Hauke, A. Eckardt, M. Lewenstein, and L. Mathey, Nat. Phys. **9**, 738 (2013).

[31] M. Aidelsburger, M. Atala, M. Lohse, J. T. Barreiro, B. Paredes, and I. Bloch, Phys. Rev. Lett. **111**, 185301 (2013).

[32] H. Miyake, G. A. Siviloglou, C. J. Kennedy, W. C. Burton, and W. Ketterle, Phys. Rev. Lett. **111**, 185302 (2013).

[33] A. Gómez-León and G. Platero, Phys. Rev. Lett. **110**, 200403 (2013).

[34] G. Jotzu, M. Messer, R. Debusquois, M. Lebrat, T. Uehlinger, D. Greif, and T. Esslinger, Nature **515**, 237 (2014).

[35] N. Goldman, G. Juzeliūnas, P. Öhberg, and I. B. Spielman, Rep. Prog. Phys. **77**, 126401 (2014).

[36] A. S. Sørensen, E. Demler, and M. D. Lukin, Phys. Rev. Lett. **94**, 086803 (2005).

[37] A. Bermudez, T. Schaetz, and D. Porras, Phys. Rev. Lett. **107**, 150501 (2011).

[38] M. Aidelsburger, M. Lohse, C. Schweizer, M. Atala, J. T. Barreiro, S. Nascimbène, N. R. Cooper, I. Bloch, and N. Goldman, Nat. Phys. **11**, 162 (2014).

[39] S. K. Baur, M. H. Schleier-Smith, and N. R. Cooper, Phys. Rev. A **89**, 051605(R) (2014).

[40] T. Oka and H. Aoki, Phys. Rev. B **79**, 081406(R) (2009).

[41] T. Kitagawa, E. Berg, M. Rudner, and E. Demler, Phys. Rev. B **82**, 235114 (2010).

[42] P. M. Perez-Piskunow, G. Usaj, C. A. Balseiro, and L. E. F. Foa Torres, Phys. Rev. B **89**, 121401(R) (2014).

[43] M. C. Rechtsman, J. M. Zeuner, Y. Plotnik, Y. Lumer, D. Podolsky, F. Dreisow, S. Nolte, M. Segev, and A. Szameit, Nature **496**, 196 (2013).

[44] N. H. Lindner, G. Refael, and V. Galitski, Nat. Phys. **7**, 490 (2011).

[45] B. Dóra, J. Cayssol, F. Simon, and R. Moessner, Phys. Rev. Lett. **108**, 056602 (2012).

[46] Z. Gu, H. A. Fertig, D. P. Arovas, and A. Auerbach, Phys. Rev. Lett. **107**, 216601 (2011).

[47] P. Delplace, A. Gómez-León, and G. Platero, Phys. Rev. B **88**, 245422 (2013).

[48] A. Gómez-León, P. Delplace, and G. Platero, Phys. Rev. B **89**, 205408 (2014).

[49] N. Goldman and J. Dalibard, Phys. Rev. X **4**, 031027 (2014).

[50] A. P. Itin and M. I. Katsnelson, arXiv:1401.0402v2.

[51] A. Eckardt and E. Anisimovas, arXiv:1502.06477v3.

[52] A. G. Grushin, Á. Gómez-León, and T. Neupert, arXiv:1503.02580.

[53] R. Blümel, A. Buchleitner, R. Graham, L. Sirko, U. Smilansky, and H. Walther, Phys. Rev. A **44**, 4521 (1991).

[54] S. Kohler, T. Dittrich, and P. Hänggi, Phys. Rev. E **55**, 300 (1997).

[55] H.-P. Breuer, W. Huber, and F. Petruccione, Phys. Rev. E **61**, 4883 (2000).

[56] D. W. Hone, R. Ketzmerick, and W. Kohn, Phys. Rev. E **79**, 051129 (2009).

[57] R. Ketzmerick and W. Wustmann, Phys. Rev. E **82**, 021114 (2010).

[58] D. Vorberg, W. Wustmann, R. Ketzmerick, and A. Eckardt, Phys. Rev. Lett. **111**, 240405 (2013).

[59] K. I. Seetharam, C.-E. Bardyn, N. H. Lindner, M. S. Rudner, and R. Gil, arXiv:1502.02664v1.

[60] T. Iadecola, T. Neupert, and C. Chamon, arXiv:1502.05047v2.

[61] A. Eckardt and M. Holthaus, Phys. Rev. Lett. **101**, 245302 (2008).

[62] M. Weinberg, C. Ölschläger, C. Sträter, S. Prelle, A. Eckardt, K. Sengstock, and J. Simonet, arXiv:1505.02657.

[63] A. Lazarides, A. Das, and R. Moessner, Phys. Rev. E **90**, 012110 (2014).

[64] L. D'Alessio and M. Rigol, Phys. Rev. X **4**, 041048 (2014).

[65] J. Dalibard, F. Gerbier, G. Juzeliūnas, and P. Öhberg, Rev. Mod. Phys. **83**, 1523 (2011).

[66] W. Zheng and H. Zhai, Phys. Rev. A **89**, 061603(R) (2014).

[67] S. Rahav, I. Gilary, and S. Fishman, Phys. Rev. A **68**, 013820 (2003).

[68] N. Goldman, J. Dalibard, M. Aidelsburger, and N. R. Cooper, Phys. Rev. A **91**, 033632 (2015).

[69] Formula (C.10) in Ref. 49 differs from our Eq. (14c) by an apparently spurious factor of 2 in front of the last triple commutator which, however, does not contribute in the present case.

[70] T. Kitagawa, T. Oka, A. Brataas, L. Fu, and E. Demler, Phys. Rev. B **84**, 235108 (2011).

[71] L. Guo, M. Liu, and M. Marthaler, arXiv:1503.03096.

[72] M. Bukov, L. D'Alessio, and A. Polkovnikov, arXiv:1407.4803v4.

[73] A. Verdeny, A. Mielke, and F. Mintert, Phys. Rev. Lett. **111**, 175301 (2013).

[74] L. D'Alessio, arXiv:1412.3481.

[75] S. Blanes, F. Casas, J. A. Oteo, and J. Ros, Phys. Rep. **470**, 151 (2009).

[76] Q. Niu and D. J. Thouless, J. Phys. A: Math. Gen. **17**, 2453 (1984).

[77] T. O. Wehling, E. Şaşıoğlu, C. Friedrich, A. I. Lichtenstein, M. I. Katsnelson, and S. Blügel, Phys. Rev. Lett. **106**, 236805 (2011).

[78] S. Kourtis, T. Neupert, C. Chamon, and C. Mudry, Phys. Rev. Lett. **112**, 126806 (2014).

[79] A. G. Grushin, J. Motruk, M. P. Zaletel, and F. Pollmann, Phys. Rev. B **91**, 035136 (2015).

[80] L. B. Shao, S.-L. Zhu, L. Sheng, D. Y. Xing, and Z. D. Wang, Phys. Rev. Lett. **101**, 246810 (2008).

[81] T. D. Stanescu, V. Galitski, and S. Das Sarma, Phys. Rev. A **82**, 013608 (2010).

[82] E. Alba, X. Fernandez-Gonzalvo, J. Mur-Petit, J. K. Pachos, and J. J. Garcia-Ripoll, Phys. Rev. Lett. **107**, 235301 (2011).

[83] N. Goldman, E. Anisimovas, F. Gerbier, P. Öhberg, I. B. Spielman, and G. Juzeliūnas, New J. Phys. **15**, 013025 (2013).

[84] E. Anisimovas, F. Gerbier, T. Andrijauskas, and N. Goldman, Phys. Rev. A **89**, 013632 (2014).